*Int. J. Heat Mass Transfer.* Vol. 24, No. 4, pp. 581–595, 1981
Printed in Great Britain

0017–9310/81/040581–15 $02.00/0


# AN EXPERIMENTAL AND ANALYTICAL STUDY OF HEAT TRANSFER IN AN ENGINE EXHAUST PORT

J. A. CATON
Texas A & M University, College Station, TX 77843, U.S.A.
and
J. B. HEYWOOD
Sloan Automotive Laboratory, Massachusetts Institute of Technology, Cambridge, Massachusetts, U.S.A.

(*Received* 11 *April* 1980 *and in revised form* 2 *September* 1980)

**Abstract**—Because of the increasing need for precise information on engine processes, this study developed and experimentally verified models for the instantaneous heat transfer in an engine exhaust port. Experimental measurements were made of the instantaneous cylinder pressure and instantaneous exhaust gas temperature for a range of engine operating conditions. The pressure measurements were used to obtain the instantaneous cylinder gas state and the temperature measurements were used to validate the heat transfer models.

The exhaust port heat transfer was dominated by jet induced large-scale fluid motion as opposed to wall-shear generated fluid motion. An analysis based on the jet velocity through the valve opening correctly estimated the heat transfer due to this large-scale motion. Models for the instantaneous exhaust port heat transfer provided excellent agreement with measurements as a function of engine operating conditions.

## NOMENCLATURE

$A_f$, flow area of exhaust port;
$C_1$, constant for developing flow in a pipe;
$C_2$, constant for pipe roughness;
$C_P$, specific heat at constant pressure;
$CA$, crank angle;
$d_e$, eddy length scale;
$D$, exhaust port or valve diameter;
$f$, cylinder residual mass fraction;
$h_C$, cylinder heat-transfer coefficient;
$h_P$, exhaust port heat-transfer coefficient;
$h_V$, exhaust valve heat-transfer coefficient;
IMEP, indicated mean effective pressure—the work per cycle over the compression and expansion strokes divided by the displaced volume;
$k$, thermal conductivity;
$K$, adjustable fit coefficient;
$l_V$, valve lift;
$L_C$, length between piston top and cylinder head;
$\dot{m}_E$, exhaust gas mass flow rate;
$\dot{m}_i$, exhaust gas mass for element $i$;
$M$, finite difference solution stability parameter;
$n$, empirical exponent for heat-transfer correlations;
N, finite difference time increment index parameter;
$Nu_C$, $= h_C L_C/k$, cylinder Nusselt number;
$Nu_P$, $= h_P D/k$, exhaust port Nusselt number;
$Nu_V$, $= h_V l_V/k$, exhaust valve Nusselt number;
$P_C$, instantaneous cylinder pressure;
$Pr$, $= \nu/\alpha$, Prandtl number;
$\dot{Q}_C$, cylinder heat-transfer rate;
$\dot{Q}_i$, exhaust port heat-transfer rate for element $i$;
$Re_C$, $= U_C L_C/\nu$, cylinder Reynolds number;
$\overline{Re}_D$, $= \bar{U}D/\nu$, average exhaust Reynolds number;
$Re_j$, $= U_j D/\nu$, exhaust jet Reynolds number;
$Re_P$, $= U_P D/\nu$, exhaust port Reynolds number;
$Re_V$, $= U_j l_V/\nu$, exhaust valve Reynolds number
$\Delta t$, finite difference time increment;
$T_C$, instantaneous cylinder gas temperature;
$\bar{T}_C$, mass-averaged cylinder gas temperature;
$T_i$, exhaust gas temperature for element $i$;
$T_P$, instantaneous port exit temperature;
$\bar{T}_P$, mass-averaged port exit gas temperature;
$\bar{T}_{PC}$, computed mass-averaged port exit gas temperature;
$\bar{T}_{PX}$, experimental mass-averaged port exit gas temperature;
$T_W$, exhaust port wall temperature;
$\bar{U}$, average total exhaust port gas velocity;
$U_C$, cylinder gas velocity;
$U_j$, Exhaust jet gas velocity through valve opening
$U_P$, exhaust port gas velocity;
$\Delta x$, finite difference spatial increment.

Greek symbols

$\alpha$, $= k/(\rho C_P)$, thermal diffusivity;
$\theta_{SR}$, spark timing relative to MBT timing;
$\nu$, kinematic viscosity;
$\rho$, gas density;
$\tau_t$, characteristic time for "wiping" process;
$\phi$, fuel–air equivalence ratio.

## INTRODUCTION

QUANTITATIVE information on heat transfer in an

engine exhaust system is important for both engine design and diagnostic efforts. For design efforts, this information permits the optimization of exhaust system devices. For diagnostic efforts, such information permits more precise extrapolation of measurements downstream of the exhaust valve to in-cylinder conditions.

Motivations for this investigation include the application of exhaust system devices such as turbochargers, catalytic converters and thermal reactors. For example, the use of turbochargers for internal-combustion engines requires accurate turbine-inlet temperatures to interpret performance characteristics. Accurate gas temperature knowledge is also useful in optimizing the location of certain catalytic elements in the exhaust system. The ideal location permits rapid warm-up without exposing the catalyst to damaging high temperatures. Another application is the oxidation of hydrocarbon species in the exhaust system of spark ignition engines [1].

This investigation was limited to the exhaust port region in the exhaust system. This region was recognized as comprising the most complex set of flow and heat transfer processes. The remaining elements of the exhaust system could be treated as either parallel or series connected plenums and pipes.

The purpose of this investigation was to model analytically the heat transfer in an exhaust port of a spark-ignited engine. To accomplish this, experimental measurements were obtained to fulfill two requirements. First, the experimental data guided the modelling effort; and, second, the experimental data verified the final heat-transfer models. The primary measured variables were instantaneous cylinder pressures and instantaneous port exit temperatures. These variables were obtained for a range of engine operating conditions.

Table 1. CFR engine specifications

| Parameter | Value |
|---|---|
| Bore (mm) | 82.6 |
| Stroke (mm) | 114. |
| Connecting rod length (mm) | 254. |
| Compression ratio | 7.24:1 |
| Coolant temperature (K) | 340±10 |
| Oil temperature (K) | 330±10 |
| Inlet mixture temperature (K) | 350±5 |
| Valve diameter (mm) | 31.8 |
| Intake Valve | |
| Opens | 10 deg after TDC |
| Closes | 34 deg after BDC |
| Exhaust Valve | |
| Opens | 150 deg after TDC |
| Closes | 20 deg after TDC |
| Fuel | Isooctane |

The overall modelling procedure included the following steps. From the measured cylinder pressures, the gas temperature and exhaust flow rate at the valve were computed using standard engine modelling techniques. The port exit gas temperature was then computed from the exhaust port heat transfer models. The computed and measured port exit temperatures were then compared as a function of time and engine operation.

## EXPERIMENTAL APPARATUS

### *Engine installation*

The spark-ignition engine was a single-cylinder Cooperative Fuel Research (CFR) engine with valve-in-head and variable compression ratio. The compression ratio was constant for these studies and determined to be 7.24:1 by a displacement measurement of the clearance volume. The CFR engine was coupled to an electric dynamometer which permitted the engine to be motored or fired at constant speed. The fuel, isooctane, and air were metered into an inlet mixing plenum which was jacketed with water and steam to hold reactant mixture temperature constant. The fuel and air supply systems were independent as contrasted to a carbureted system where the fuel flow rate depends on the air flow rate. Table 1 lists the major engine parameters.

Cylinder pressure was measured by a water-cooled piezoelectric pressure transducer in conjunction with a charge amplifier. Testing and evaluation of the pressure signal as recommended by Lancaster *et al.* [2] indicated satisfactory operation. This evaluation verified transducer performance as well as crank angle phasing, clearance volume and reference pressure. A rotary pulse generator and appropriate electronics were used to supply a signal pulse every crank angle for data acquisition. The exhaust system consisted of a short straight pipe from the exhaust port and into an exhaust surge tank. The exhaust gas flowed from the engine into the surge tank and then into the laboratory exhaust trench. The instantaneous exhaust pressure was measured by a water cooled strain gauge. A fine chromel-alumel thermocouple was installed in the pope wall near the inner surface.

### *Fine-wire resistance thermometer*

The measurement of instantaneous exhaust gas temperatures for guiding the early modelling effort and for verifying the final heat-transfer models required a temperature transducer with a relatively high frequency response. In addition, the need to detect possible fluid stratificqtion required a transducer with spatial discrimination across the exhaust cross-section. A suitable temperature transducer which satisfied these requirements was a fine-wire resistance thermometer [3–5].

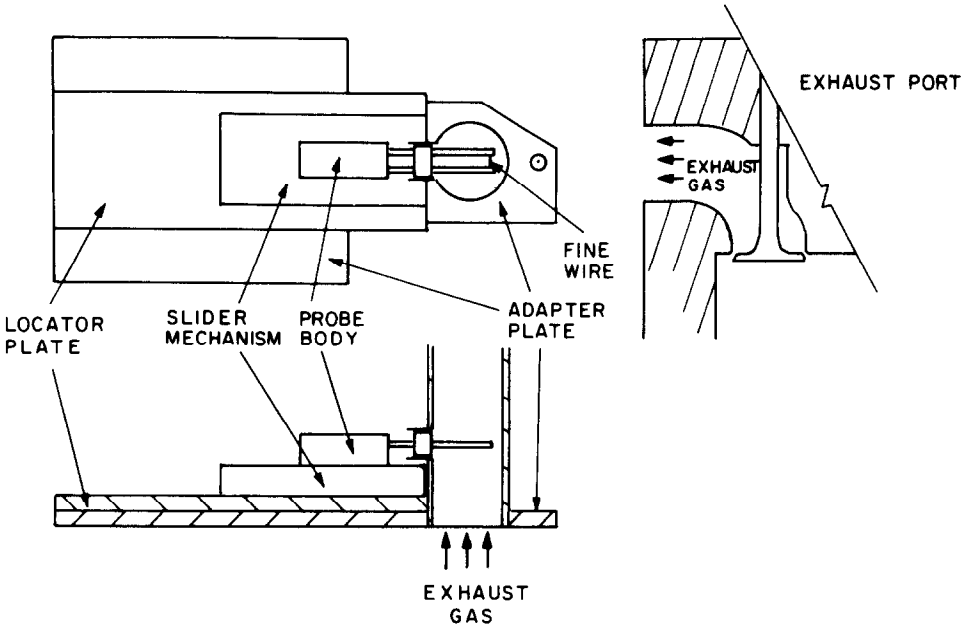


FIG. 1. Schematic diagram of the temperature probe installation and exhaust port geometry.

The fine-wire resistance thermometer employed in this investigation used a 9 $\mu$m dia. tungsten wire 8 mm long in a constant current (5 mA) circuit. The wire temperature was related directly to the wire resistance which was determined by measuring the voltage drop. To determine the wire temperature–resistance relation, steady-state calibration tests were conducted in an electric furnace for several wire specimens. Benson and Brundrett [3] present a detailed analysis of the errors associated with the use of a fine-wire resistance thermometer to measure instantaneous exhaust gas temperatures.

Figure 1 shows the temperature probe installation with respect to the engine geometry. The temperature probe was mounted on a precision slider and the complete unit was installed on the exhaust port of the CFR engine. A small access port on the side of the exhaust pipe permitted the probe to be inserted into the exhaust gas. This arrangement allowed convenient insertion and removal while maintaining a nearly leak-proof entry. The exhaust gas temperatures were measured in a cross-sectional plane 11.4 cm downstream of the valve face.

*Data acquisition system*

Since simultaneous cylinder pressure and exhaust gas temperature measurements were required, an on-line digital data acquisition system was employed for these experiments. The acquisition system used a minicomputer with an analog-to-digital converter. The crank angle pulses were used to trigger the analog-to-digital conversion via a Schmidt trigger and a single signal pulse (marker) once every two engine revolutions was used to initiate a set of conversions. Ensemble averages and standard deviations were computed for the cylinder pressures and exhaust gas temperatures from the total number of engine cycles sampled.

## EXPERIMENTS

*Test matrix and procedure*

Table 2 lists the test matrix for the engine operating conditions. These engine conditions were selected to minimize the mean exhaust temperature as well as permit investigation of the major engine variables—load (defined by indicated mean effective pressure, IMEP), engine speed, equivalence ratio and spark timing. Low exhaust temperatures were required

Table 2. Test matrix for engine operating conditions

| Parameter varied* | IMEP (kPa) | Speed (RPM) | $\phi$ | $\theta_{SR}$ (degrees) |
|---|---|---|---|---|
| BASE (B) | 414 | 1000 | 1.2 | -10 |
| IMEP (A) | 276 | 1000 | 1.2 | -10 |
| (C) | 621 | 1000 | 1.2 | -10 |
| SPEED | 414 | 1300 | 1.2 | -10 |
| (D) | 414 | 1600 | 1.2 | -10 |
| $\phi$ | 414 | 1000 | 1.0 | -10 |
| | 414 | 1000 | 1.4 | -10 |
| $\theta$ | 414 | 1000 | 1.2 | -20 |
| SR | 414 | 1000 | 1.2 | 0 |
| | 414 | 1000 | 1.2 | +15 |

* Where appropriate the "case" letter is listed in parentheses.

to minimize the oxidation of the tungsten wire of the resistance thermometer [6].

The experimental procedure was first to establish stable engine operation at the preselected test conditions. The resistance thermometer was calibrated at the steady-state ambient temperature. This adjusted the measurement for any slight differences due to fabrication, electronics or oxidation from a prior measurement. This adjustment was generally on the order of $\pm 5\%$. The temperature probe was then inserted into the exhaust port and data acquisition was initiated. The engine operating variables and exhaust gas compositions were logged. The simultaneous cylinder pressures and exhaust gas temperatures were recorded via the data acquisition system for a preselected number of engine cycles. This data acquisition process typically required about 5 min for 10 or 20 engine cycles. The majority of this time was used for necessary preliminary data processing and storage, and not actual data acquisition.

After the data acquisition and processing was completed the temperature probe was removed from the exhaust port. The calibration of the fine wire was then checked for indications of any tungsten oxidation. If no change was detected, the measurement was considered acceptable. If oxidation had occurred, the wire was recalibrated and the procedure repeated. Highly oxidized wires ($\sim 50\%$ increase in original resistance) were replaced. The repeatability of the exhaust gas temperature measurements for a specific probe and a particular engine setting was excellent. For different probes and different days, the repeatability was within $\pm 5\%$ which is indicative of measurement and engine operation uncertainties.

*Experimental results*

To explore the quality of the experimental data, cyclic variations of the cylinder pressure and exhaust gas temperature were examined. Cyclic variations of cylinder pressure were expected and the maximum standard deviation as a percentage of the mean pressure was generally of order $10\%$ which is typical for normally operating spark-ignition engines. For the base case, the maximum cylinder pressure variation was $6\%$ while the maximum exhaust gas temperature variation was $3\%$. In general, the cyclic variation was

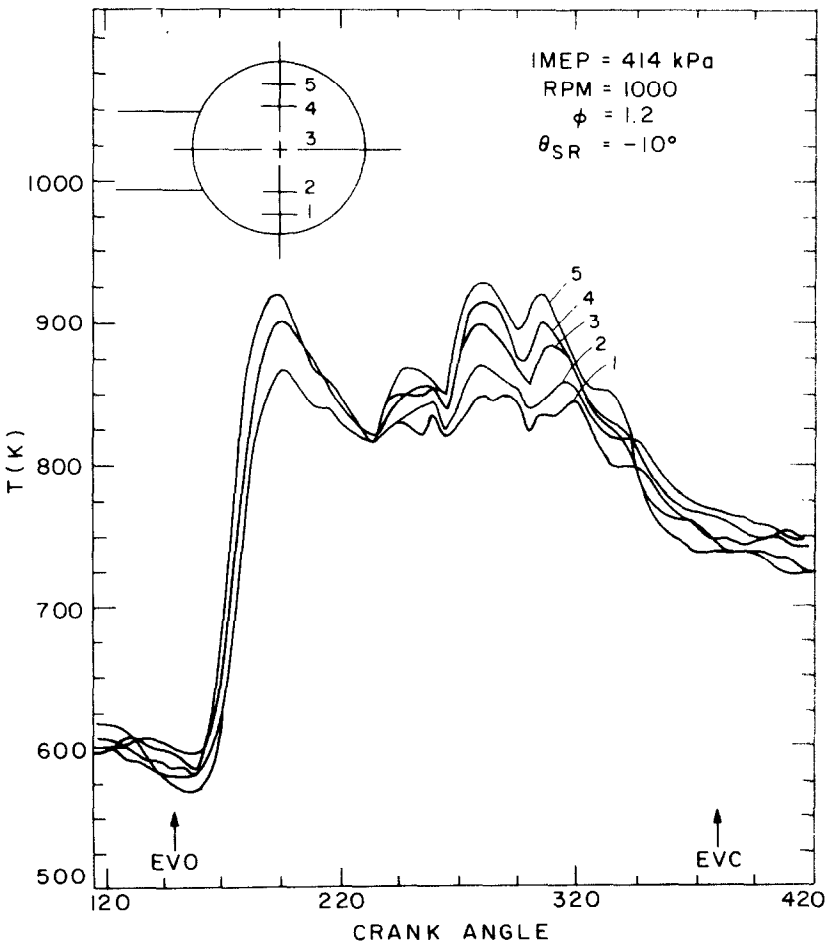


FIG. 2. Measured instantaneous port exit gas temperatures as a function of crank angle for five locations on the vertical diameter.

minimal; and, therefore, 10 or more engine cycles were deemed adequate to determine representative ensemble averages.

Of particular interest to this investigation was the degree of spatial nonuniformity of the exhaust gas temperature at the measurement plane. Figure 2 illustrates the results for a vertical traverse for the base engine operating condition. In general, the character of the exhaust gas temperature with crank angle was similar at all locations in the cross-sectional plane [6]. Furthermore, during the high temperature portion of the measurement the variation was at most $\pm 5\%$ and at any time the maximum variation was less than $\pm 8\%$

The variation was systematic: in the horizontal traverse the temperature continually decreased from the outer wall to the location near the probe entrance and in the vertical traverse the temperature continually decreased from top to bottom. The center line temperature was an approximate spatial average of the temperatures at all locations. In the following sections, only the exhaust gas temperatures at the center line are reported.

For verification of the exhaust port heat transfer model, exhaust gas temperature data was obtained as a function of engine operating variables. Although tungsten wire oxidation limited the range of engine operating variables, results were acquired for variations in engine load, speed, equivalence ratio and spark timing. To maintain relatively low exhaust temperatures, each variable was independently changed from the base condition. This data is examined in a subsequent section.

## ENGINE CYLINDER CONDITIONS

Gas temperatures and mass flow rates at the exhaust valve were required to compute the port exit temperature for comparison with the measured temperatures. Since these parameters are difficult to measure, standard simulation procedures [7] were used to compute these parameters from the measured cylinder pressures. For this investigation, the simulation procedures were simplified because the thermodynamic state of the gas in the cylinder was required only during the exhaust valve open period. This meant that calculations for the engine intake, compression and combustion processes were not needed. The calculations, therefore, were started at the instant prior to exhaust valve opening and, from the ideal gas law, the initial cylinder gas temperature was calculated from known quantities.

The engine cylinder was modelled as a variable volume, open control system with mass flow rates through the exhaust valve, with heat transfer to the cylinder boundaries and work transfer to the piston. The gas mixture was assumed homogeneous during the exhaust valve open period with cylinder temperature and pressure a function of time and not space. Additionally, the gas mixture composition was determined from an element balance and the measured equivalence ratio, assuming only major species were present [8, 9]. The individual species were assumed to satisfy the ideal gas relationship. Average thermodynamic properties of the gas were calculated using a mole fraction weighted average of the individual specific properties. For exhaust temperatures above 1000 K, thermodynamic properties were determined from approximated data which allowed for chemical dissociation [10]. The first law of thermodynamics was used to determine the instantaneous state of the cylinder gas. This energy conservation equation was expanded to give a first order differential equation for the cylinder temperature as a function of known quantities [8].

A turbulent "boundary-layer" model was used for the cylinder heat-transfer process. An empirical heat-transfer correlation for turbulent flow over a flat plate [11] was employed

$$Nu_C = 0.037 Re_C^{0.8} Pr^{0.33}. \quad (1)$$

This expression was increased by a factor of two to allow for heat-transfer augmentation due to regions of developing flow and for roughness from deposits on the upper cylinder areas. The characteristic velocity (based on the piston area) was the larger of either the instantaneous mean exhaust flow or piston speed. The characteristic length was the instantaneous distance between the piston top and cylinder head.

A common alternative for the cylinder heat transfer is an expression developed by Woschni [12] for diesel engines. Besides being based on diesel engines, this expression had the disadvantage of using the mean piston speed with an experimentally determined augmentation factor of 6.18 for the exhaust stroke. An augmentation factor greatly different than unity indicates that the fundamental processes were not properly characterized. For general engine computations, this discrepancy is not significant; but, for the purposes of the present investigation, this lack of detail is significant.

Flow rates through the exhaust valve were calculated from one-dimensional compressible flow equations for quasi-steady, adiabatic and isentropic flow [7, 13]. The isentropic assumption was relaxed by the use of a discharge coefficient. Empirical data based on valve lift to diameter ratios were used to determine the valve discharge coefficient [6, 14].

## METHODOLOGY OF EXHAUST PORT HEAT-TRANSFER MODELLING

### *Overview and assumptions*

No instantaneous heat-transfer correlation for flow in an engine exhaust port was available; and, furthermore, available heat-transfer correlations for other flows could not be simply extended to flow in an engine exhaust port. A detailed, time-dependent model, therefore, was developed for the heat transfer due to flow in an exhaust port.

The modelling approach was to develop fundamental sub-models for the dominant heat-transfer modes in an exhaust port. A more precise approach (e.g.

solutions to the governing differential momentum, energy and mass equations) was precluded because of complexities of the periodic, turbulent exhaust gas flow through a time-dependent opening poppet valve into an obstructed, curved passage. The sub-model approach was selected as a practical engineering alternative.

Several general assumptions and approximations were required in formulating the heat-transfer models. The flow processes in the exhaust port were approximated as quasi-steady and one-dimensional. Axial temperature gradients were included and the gas properties were assumed to be uniform at any cross-sectional plane. Heat transfer was assumed to be perpendicular to the surface and circumferentially uniform. The exhaust gas was assumed to satisfy the ideal gas relationship and to have thermodynamic properties determined by the previously discussed methods. Other specific assumptions and approximations are discussed as required in the following sections.

Although the heat transfer was transient, the time variation of port wall temperature was neglected and a time-mean value was used. Since the port wall temperature variation was small ($\sim 10$ K) relative to the temperature difference ($\sim 500$ K), this approximation was valid. The time-mean port wall temperature for the water-cooled region of the port was estimated to be 350 K. Average temperature difference between water and gas side of port walls was estimated to be 10 K. For the uncooled downstream region of the port, the time-mean temperature was estimated to be 500 K which was the average temperature of a small (dia. = 0.8 mm) thermocouple located near the inside wall. The valve and valve stem time-mean surface temperature was assumed to be 500 K [15].

The flow was initially approximated as plug (or slug) flow which is an adequate model for fully developed turbulent flow in a pipe. For most of the exhaust port, therefore, plug flow is a valid approximation. For the flow near the valve, back-mixing occurs and a plug flow assumption is less adequate. For the flow near the valve, a simple mixing model was used. The details of this mixing model are described in [6].

*Dominant modes of heat transfer*

As previously noted, the modelling approach was to develop fundamental sub-models to describe the dominant heat-transfer processes in an engine exhaust port. These sub-models are either adapted empirical correlations or simple expressions derived from an order-of-magnitude analysis. These sub-models are described separately in this section for convenience. In subsequent sections, these sub-models are examined independently and in combination as descriptions of the exhaust port heat-transfer process.

*Pipe flow.* Since the exhaust port is geometrically similar to a curved pipe, an initial consideration was the empirical correlation for heat transfer for turbulent flow in a pipe [11]

$$Nu_P = C_1 C_2 0.023 Re_P^{0.8} Pr^{0.4}. \quad (2)$$

The empirical constants, $C_1$ and $C_2$, account for developing flow and pipe roughness [11, 16]. These constants were a function of exhaust port Reynolds number and axial position [6]. The use of this correlation implies that the heat-transfer process is governed by the turbulence generated by wall shear stresses. This wall-generated turbulence may be significant for certain portions of the flow, but clearly other sources of turbulence also exist.

*Large-scale motion.* For low valve lifts, the flow into the exhaust port is approximately a convergent, conical jet issuing into a relatively large volume [14] Exhaust flow visualization experiments [17, 18] indicated that the high jet velocities produce large-scale turbulent fluid structures in the exhaust port. The scale of the resulting motion was approximately half of the port diameter. This motion is not accounted for by the wall-generated turbulence; but this motion would result in increased heat-transfer rates. No empirical or analytical correlation existed in the literature for the heat transfer produced by such jet-induced motion; hence, an analytical expression which incorporated the gross effect of the motion was developed. In this order-of-magnitude analysis [19] the large scale motion is approximated as a series of eddies with diameter equal to half the port diameter, local velocity equal to the instantaneous jet velocity and gas temperature equal to the local instantaneous temperature. These eddies are assumed to "wipe" the wall surface for a length equal to their diameter. Figure 3 schematically illustrates these features.

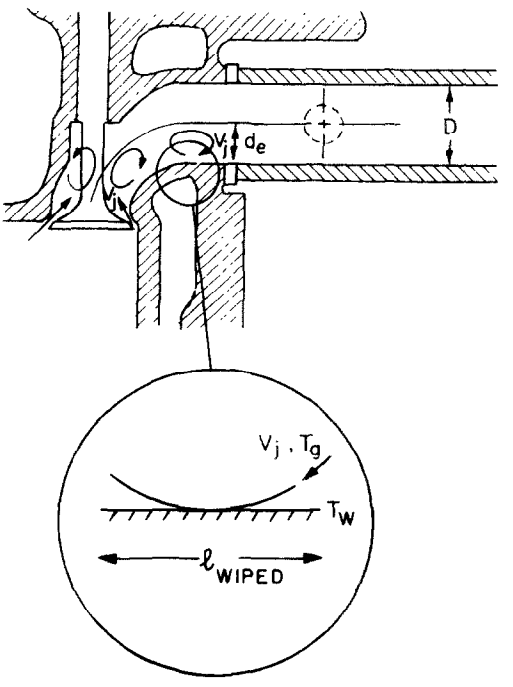


FIG. 3. Schematic illustration of the large-scale motion heat transfer.

During the "wiping" process, higher temperature gas from the bulk flow is brought into contact with the lower temperature gas near the surface. An analogy was developed between this process and the unsteady heat conduction of a semi-infinite solid with a step change in surface temperature. In the wiping process, the initial temperature, $T_i$, is approximated as the wall temperature and the surface temperature, $T_0$, is suddenly raised to the local mean bulk gas temperature. The solution for the surface heat transfer [20] at any time, $t$, is

$$q_0 = kA(T_0 - T_i)/(\pi\alpha t)^{0.5}. \quad (3)$$

The average heat flux during the time, $\tau_t$, that the eddy "wipes" the surface is

$$q_{avg}/A = \frac{1}{\tau_t}\int_0^{\tau_t} q_0\,dt = 2k(T_0 - T_i)/(\pi\alpha\tau_t)^{0.5}. \quad (4)$$

The characteristic time, $\tau_t$, for this process is

$$\tau_t = l_{wiped}/\text{velocity} = (D/2)/V_j. \quad (5)$$

A non-dimensional expression was obtained from the Nusselt number definition,

$$Nu_P = h_P D/k = (q/A)_{avg} D/(k\,\Delta T). \quad (6)$$

Combining equations (4)–(6),

$$Nu_P = \{D/(k\,\Delta T)\}\{2k\,\Delta T/[(\pi\alpha D)/(2V_j)]^{0.5}\} \quad (7)$$

Rearranging and introducing definitions,

$$Nu_P = (8Re_j Pr/\pi)^{0.5}. \quad (8)$$

The final relation, then, accounts for the exhaust port heat transfer resulting from the large-scale motion which was generated by the high velocity jet. For this relation to be valid, the eddy turn-over time must be less than the eddy's port residence time. This condition was satisfied in the current study.

*Valve.* Heat transfer to the valve back and valve stem was also treated. The mean flow through the valve opening was assumed to be directed at the valve stem. At least locally, then, stagnation point flow was anticipated with corresponding high heat-transfer rates. An empirical [21] correlation for two-dimensional jet impingement was adapted to model the mean heat transfer. This correlation was derived from an experiment which consisted of flow from a slot directed at a perpendicular surface.

For the jet impingement experiment, the correlation obtained was [21],

$$Nu_B = hB/k = 1.2Re_e'^{0.58}(B/Z_N)^{0.62} \quad (9)$$

where,

$$Re_e' = u_e B/\nu \quad (10)$$

and $u_e$ was the exit velocity. To adapt this correlation to the valve/port geometry, the following approximations were made. The slot width, $B$, was approximated as the valve lift, $l_V$. The distance between the jet origination and termination points, $Z_N$, was approximated as half the valve diameter. These substitutions result in the following expression,

$$Nu_V = h_V l_V/k = 1.2Re_V^{0.58}(2l_V/D)^{0.62}. \quad (11)$$

*Exhaust valve closed period.* During the exhaust valve closed period, heat transfer occurs between the exhaust gas and port surfaces mainly because of the fluid motion which perisists after the exhaust valve closes. Since this residual motion is a strong function of the exhaust system configuration and since the heat transfer during the valve closed period is typically less than 10% of the total port heat transfer, a simple model for the exhaust valve closed period was deemed sufficient.

The heat transfer during the exhaust valve closed period was assumed to be primarily the result of wall-generated turbulence and hence the empirical correlation for heat transfer in a pipe [11] was used [equation (2)]. In this case, the velocity of the residual motion was approximated by the average velocity for the time period of the complete four stroke engine cycle (two revolutions). This is a pseudo-exhaust flow rate since the valve is closed for roughly two-thirds of the total time. Even though the Reynolds numbers during the valve closed period are generally low, the correlation for turbulent flow was used because the fluid motion is highly unstable due to flow reversals, thermal gradients and external vibrations.

*Additional considerations.* Three additional considerations were determined to have minimal effect on the heat transfer in an engine exhaust port. For turbulent flow, studies [23] indicated that the effect of tube curvature on total heat transfer was negligible for the geometry of typical exhaust ports. In addition, Rush [24] demonstrated that the heat transfer was not altered for exhaust ports of different curvature.

The effect of flow pulsations on the heat transfer has been studied [25, 26], but no direct interpretation applies these results to the engine exhaust case. Furthermore, the Reynolds number and frequency ranges were outside the ranges of the current study. Other investigators [27] have also assumed the effects of flow pulsations on heat transfer to be negligible in exhaust systems.

Radiation from the water vapor and carbon dioxide of the exhaust gas was estimated as negligible because the gas emissivities and gas temperatures were relatively low in this study. Radiation from surfaces was assumed negligible because of the relatively small wall temperature differences and because of the low absolute wall temperature levels.

*Problem formulation and solution*

To obtain the gas temperature as a function of time and space in the exhaust port, a first law thermodynamic analysis was developed. As depicted in Fig. 4, the exhaust port was modelled as a series of open control volumes at constant pressure with mass flow rates in and out. Heat loss from the control volumes but no work transfer was included in the analysis.

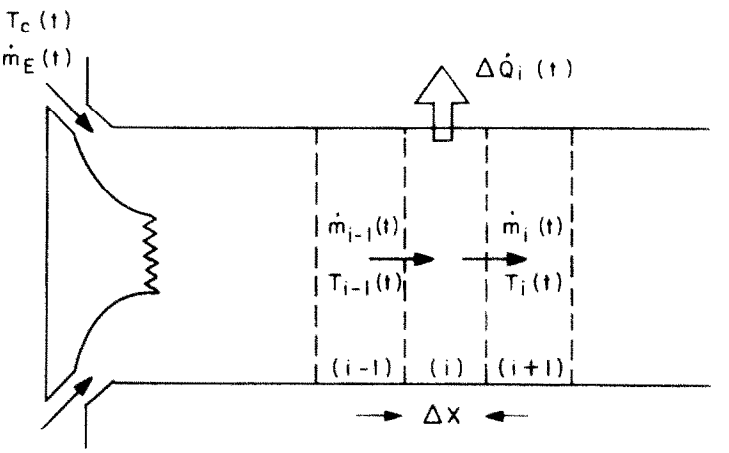


FIG. 4. Schematic illustration of the finite difference solution algorithm for the exhaust port.

Combining the energy and mass conservation equations produced an expression for the rate of change of temperature in the control volume,

$$\dot{T} = (1/mC_P)[-\dot{Q} + \dot{m}_1 C_P(T_1 - T)]. \quad (11)$$

The mass flow out is

$$\dot{m}_0 = \dot{m}_1 + m\dot{T}/T. \quad (12)$$

Equations (11) and (12) constitute the problem formulation in terms of known quantities in a differential form. The solution of these equations is presented in the remainder of this section.

A finite difference numerical technique [28, 29] was selected to solve the above equations. Using Taylor series expansions, equation (11) was cast into a difference form,

$$T_i^{n+1} = T_i^n + (1/M)[(T_{i-1} - T_i) - \Delta Q_i/(m_{i-1}C_P)] \quad (13)$$

where,

$$M = \rho_i A_f \Delta x/(\dot{m}_{i-1}\Delta t). \quad (14)$$

$M$ is a parameter which relates to the solution stability [6, 29]. At any time, from mass conservation,

$$(\dot{m}_1)_i = (\dot{m}_0)_{i-1}. \quad (15)$$

This "marching" solution, therefore, is based on results from previous time steps and prior upstream elements. For the majority of the calculations, the exhaust port was divided into 10 elements (i.e. $\Delta x = 1.14$ cm) resulting in a time step of one-half crank angle degree (i.e. $\Delta t = 0.083$ ms at 1000 rev/min).

To perform the computations, boundary and initial conditions were required. The boundary conditions were the flow rate and gas temperature exiting the cylinder and, hence, entering the first element in the exhaust port. The initial flow rate in the port was zero. The initial gas temperatures for each element were obtained from a preliminary calculation based on assumed gas temperatures. The final result of this preliminary calculation was the actual initial gas temperatures which were then used in a second (and final) calculation. Two iterations, therefore, were sufficient for convergence.

*Illustrative results and comparison*

This section describes the results of a complete set of calculations for the base engine operating condition. For these calculations, a detailed time-period model of the exhaust port heat transfer was used. This model is fully explained in the next section.

Figure 5 shows the complete set of measured and calculated time-dependent variables for the base engine condition. At the top of the figure is the calculated exhaust mass flow rate. The exhaust blowdown period began at exhaust valve opening ($CA = 150°$) and ended at about $CA = 200°$; and, this was then followed by the displacement flow period. The measured cylinder pressure decreased from about 180 kPa at the time of valve opening to a mean valve of about 100 kPa during the displacement flow period. Superimposed on the mean value of the cylinder pressure during the displacement period was a small amplitude, high frequency pressure fluctuation. This fluctuation relates to the pressure wave dynamics of the exhaust system [6]. Since the calculations were based on a quasi-steady assumption, the mean cylinder pressure during the displacement period (dashed horizontal line) was used.

Also shown in Fig. 5 is the calculated cylinder temperature which decreased from about 1200 to 900 K for this case. The remaining curves are the measured (dashed curve) and the computed (solid curve) port exit exhaust gas temperature. After the exhaust valve opens, the port exit gas temperature increased (following a delay of about 15°) from about 600 to 900 K. The gas temperature decreased from this peak until about $CA = 240°$ and then increased slightly until about $CA = 320°$. From this time ($CA$

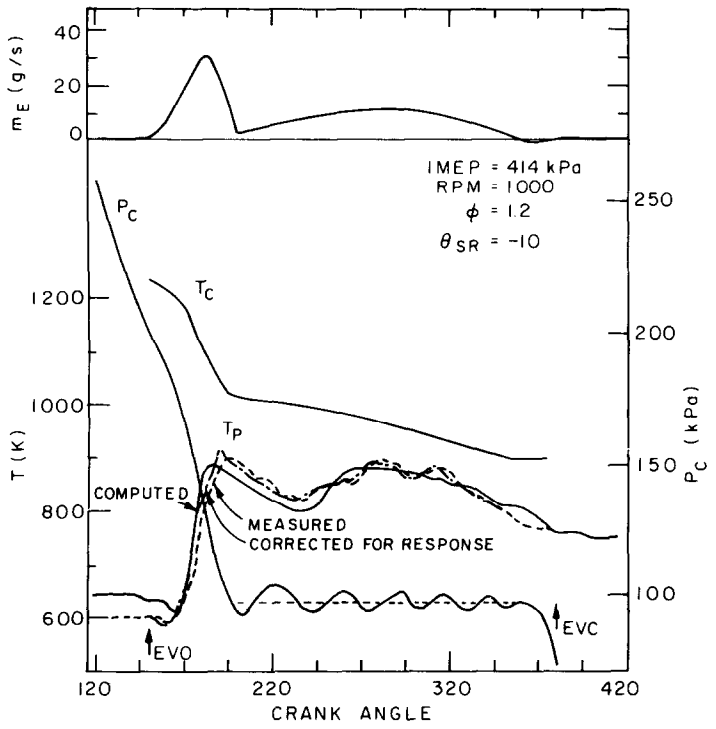


FIG. 5. Measured and computed time-dependent variables for the base engine operating conditions as a function of crank angle.

= 320°), the port exit gas temperature continually decreased through the time of exhaust valve closing ($CA$ = 380°) to the time of exhaust valve opening of the next engine cycle.

Between crank angles of 240° and 320°, superimposed on the mean port exit temperature is a high frequency temperature fluctuation which corresponded closely to a time-shifted version of the cylinder pressure fluctuation. Calculations based on an isentropic compression of the cylinder gas indicated a similar time-shifted temperature fluctuation at the port exit; but accounted for only about one-half of the temperature fluctuation amplitude. The remaining part of the amplitude of the temperature fluctuation may be a result of the quasi-steady assumption. Since the calculations were based on this quasi-steady assumption, computed port exit gas temperature should be compared to the mean of the fluctuations of the measured gas temperature.

The agreement between the computed and measured port exit exhaust gas temperatures was good. This agreement is explored more fully in the next section. The temperature measurement included a small, but finite, response error. This response error and an estimated corrected port exit temperature were determined [6] and Fig. 5 also shows this corrected temperature. The correction was small and, furthermore, resulted in better agreement between the corrected measurement and the computed instantaneous gas temperature. Because this correction was small and because of the uncertainties associated with the correction, the temperatures reported in this investigation are the measured values and not the corrected values.

## MODEL DEVELOPMENT, VALIDATION AND DISCUSSION

As previously discussed, the validation of the exhaust port heat-transfer model involved a comparison of measured and predicted port exit temperatures. For simplification, only four of the most significant engine conditions are used at this time. These four engine conditions are listed in Table 2 and are denoted as cases *A*, *B*, *C* and *D*. The other engine conditions did not alter the comparison.

As a preliminary evaluation, the individual submodels are compared in similar non-dimensional form. For a Prandtl number of 0.65, the following expressions were obtained for the correlations applicable during the exhaust valve open period:

Pipe flow* $Nu = C_1 C_2 0.0194 Re_P^{0.8}$ (16)

* The constants $C_1$ and $C_2$ were not adjustable and were obtained from the literature [11, 16] for turbulent flow in a pipe. These constants were a function of exhaust port Reynolds number and axial position [6].

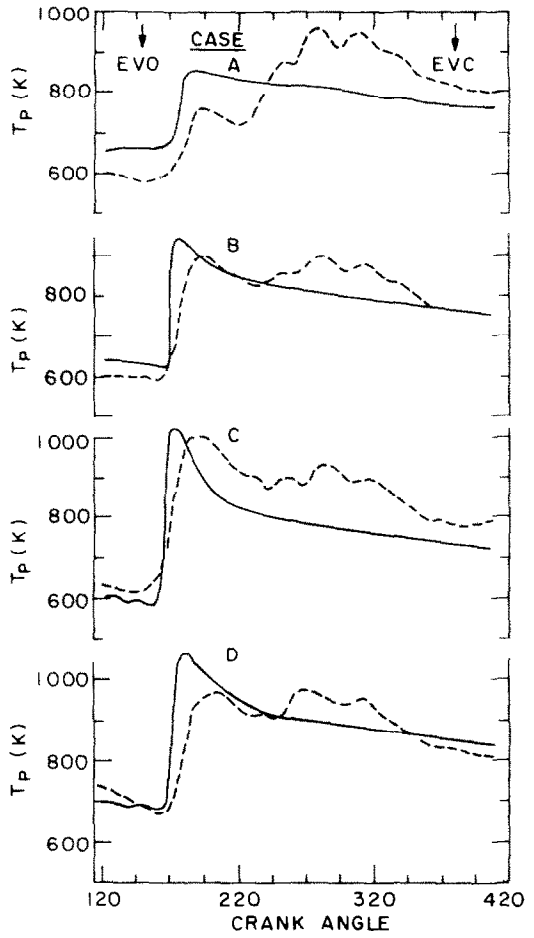


FIG. 6. Pipe flow correlation: computed (——) and measured (– – – –) port exit gas temperatures as a function of crank angle for four engine conditions.

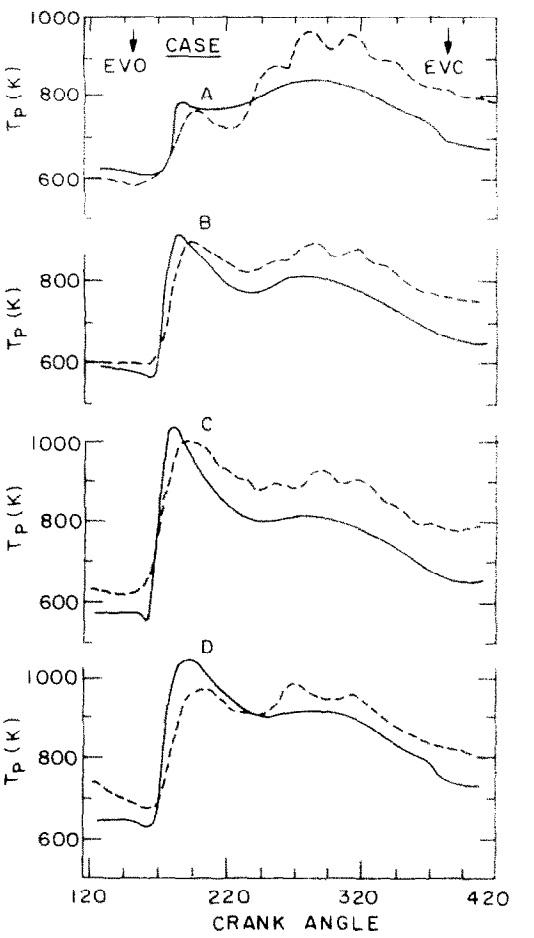


FIG. 7. Large-scale motion correlation: computed (——) and measured (– – – –) port exit gas temperatures as a function of crank angle for four engine conditions.

Large-scale motion

$$Nu = 1.29Re_j^{0.5}. \tag{17}$$

Valve impingement

$$Nu = 1.84Re_V^{0.58}(D/l_V)^{0.2}. \tag{18}$$

Empirical $Nu = K\,Re_j^n$. (19)

The correlations for large-scale motion [equation (17)] and valve impingement [equation (18)] are similar, while the correlation for pipe flow is markedly different. The fourth correlation [equation (19)] represents a purely empirical fit to the data. The exponent, $n$, was expected to range from 0.5 to 0.8 as suggested by the phenomenological sub-models [equations (16), (17) and (18)].

*Simple models*

As an initial model of the exhaust port heat transfer, single correlations were applied for the entire exhaust valve open period. Two phenomenological sub-models [correlations for pipe flow, equation (16), and for large scale motion, equation (17)] and the empirical sub-model, equation (19), were examined. A coefficient was inserted in the correlation as a multiplier constant to fit the data. This constant was expected to be of order unity if the fundamental processes were modelled correctly.

The procedure of adjusting the fit coefficient involved several considerations. The best fit was deemed to be a close match between the predicted and measured port exit temperatures at all times. This meant that no single average (e.g. mass-weighted) was a consistent criteria. For instance, the mass-weighted average may indicate close agreement but the actual difference between the predicted and measured temperature may be large during a period when the flow rate was low. For these reasons, the procedure was to select the fit coefficient with the constraint that all operating conditions were similarly matched. The selection of the fit coefficient was, in general, a compromise between under predicting the heat transfer for the high engine speed case and over predicting for the high engine load case.

The first simple model examined for the exhaust port heat transfer was the correlation for pipe flow [equation (16)]. Correlations of this form have been

used by several previous investigators [13, 27, 30, 31] to describe the heat transfer in exhaust ports. Figure 6 illustrates the results for the computed (solid curve) and measured (dashed curve) port exit temperature as a function of crank angle for the four cases. For this calculation, the fit coefficient was 2.2. The comparison between the computed and measured results indicated poor agreement in the time-dependent temperature profile, although approximate agreement was obtained for the average temperature. Because of the lack of agreement in the temperature profiles and because of the non-unity coefficient, the proper physics have probably not been included.

The next simple model examined for the exhaust port heat transfer was the correlation for the large-scale motion [equation (17)]. In this case, the fit coefficient was 1.2 which is of order unity and indicates that the proper physics are represented by the large-scale motion correlation. This is further supported by the results presented in Fig. 7. The predicted (solid curve) port exit temperature profiles demonstrated better agreement with the measured (dashed curve) temperature profiles as well as better agreement for the average temperature.

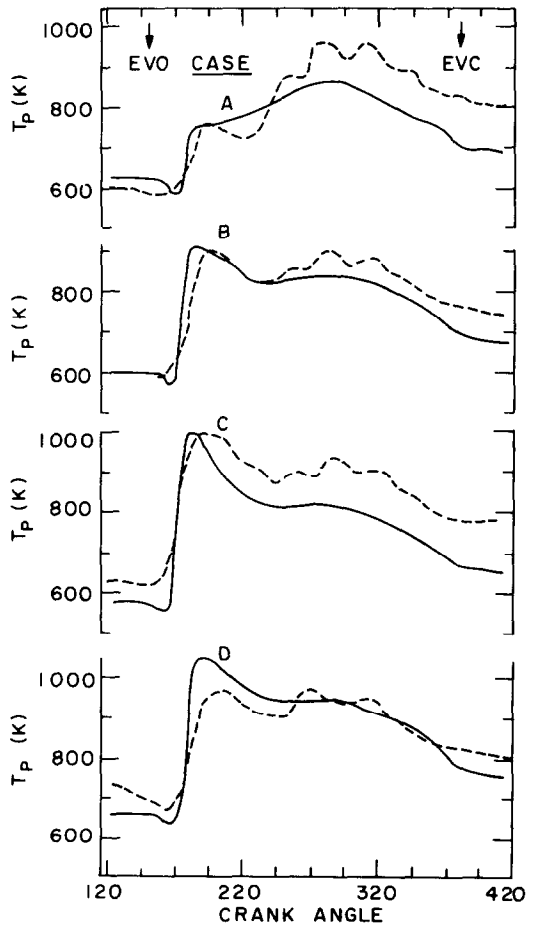


FIG. 8. Empirical large-scale motion correlation: computed (——) and measured (– – – –) port exit gas temperatures as a function of crank angle for four engine conditions.

Encouraged by the success of the large-scale motion correlation, a third correlation [equation (19)] was examined which incorporated the same functional relationship. In this empirical correlation, the exponent, $n$, was varied as well as the coefficient, $K$, to fit the data. This fit resulted in $n = 0.6$ and $K = 0.35$ (since this was a purely empirical fit, lack of unity for the coefficient has no meaning). Figure 8 shows the predicted port exit temperatures. Compared to the previous large-scale motion correlation, this empirical model resulted in some improvement in the prediction of the port exit temperatures.

The valve impingement sub-model [equation (18)] could not be evaluated alone because this correlation is applicable only to the valve back and stem surface areas and requires an additional sub-model to describe the heat loss to the port walls. The large-scale motion correlation [equation (17)] was selected to represent the heat transfer to the port walls. Using a fit coefficient of 0.8 for the large-scale motion correlation resulted in the valve impingement sub-model matching the data with a coefficient of 0.5. This value is of the right order because the correlation adapted was for stagnation point flow and, clearly, not all of the flow directed at the valve is of this character. Since the data did not differentiate between the large-scale motion and valve impingement sub-models and since the degree of stagnation flow near the valve is unknown, the valve impingement sub-model was not incorporated in the final heat transfer models.

*Time-period model*

Up to this point, single heat-transfer correlations were used for the total time of the exhaust valve open period. While this resulted in good agreement between measured and computed port exit exhaust gas temperatures, these models over-predicted the heat loss during the displacement flow period. Since no single mode of heat transfer necessarily dominates during the entire valve open period, combinations of the previously described sub-models were considered. This section describes the development and validation of a model which utilized different sub-models during different time periods.

To construct this time-period model, flow patterns in the exhaust port were identified with specific times during the valve open period. The heat transfer sub-model best associated with that particular flow pattern was then assigned to that time period. Results by Tanaka [17] and Annand and Row [14] suggested that two distinct flow patterns exist for the flow into an exhaust port. These two flow patterns are determined by valve lift. For low lifts, the exhaust gas flows into the port as a convergent, conical jet. At high lifts, the flow is a free jet coaxial with the valve stem. The recommendation [14] for the transition between these two flow regimes was a lift/diameter ratio of 0.2. This was based on measurements which indicated a decrease in the discharge coefficient for a lift/diameter ratio greater than about 0.2.

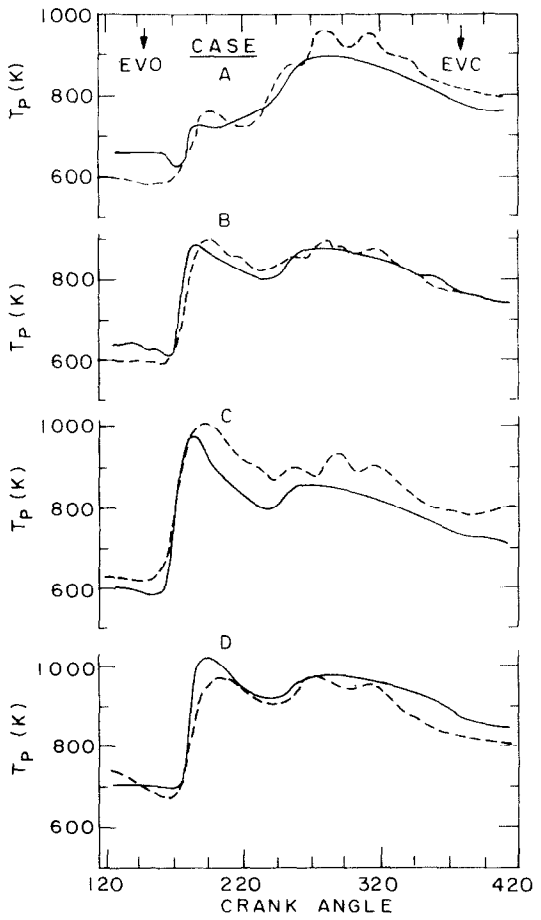


FIG. 9. Time-period correlation: computed (——) and measured (– – – –) port exit gas temperatures as a function of crank angle for four engine conditions.

From the assumed flow character, the appropriate sub-models for the time-period model were assigned. The results of the simple models [equations (17) and (19)] indicated that the heat-transfer correlation based on the large-scale motion dominated during, at least, the initial flow period. This is consistent with the low valve lift flow pattern; and, hence, the empirical large-scale motion sub-model was assigned to the first period.

The first period was terminated at $CA = 240°$ which corresponded to a valve lift/diameter ratio of 0.22. The selection of a lift/diameter ratio of 0.22 for the transition between the two flow patterns was based on the best agreement with the measured temperatures and is close to the value of 0.20 recommended by Annand and Roe [14]. Since the transition is gradual, no single value is necessarily correct.

After the first period, the flow is more coaxial and, therefore, more like turbulent pipe flow. Between $CA = 240°$ and $CA = 310°$, therefore, the pipe flow sub-model was assigned to the second period. At $CA = 310°$, the lift/diameter ratio is 0.19 which, again, is close to the recommended value.

For the final period, from $CA = 310°$ to exhaust valve closure, the flow pattern suggests that the large-scale motion again dominates. In this time period, however, the cylinder pressure is approximately equal to the exhaust pressure and less turbulence was anticipated. The large-scale motion correlation (equation (17)] obtained from the order-of-magnitude analysis was assigned to the final flow period. As with the simple models, the sub-model for the exhaust valve closed period was used for the fourth time period.

Table 3. Time-period exhaust port heat transfer model specifications

| Period | $L_v/D$ | Sub-model |
|---|---|---|
| Initial | $\geq 0.22$ | $Nu_1 = K_1 Re_j^n$ |
| Intermediate | Opening, $\geq 0.22$<br>Closing, $\geq 0.19$ | $Nu_2 = K_2\{0.0194\ C_1 C_2 Re_D^{0.8}\}$ |
| Final | $< 0.19$ | $Nu_3 = K_3\{1.29\ Re_j^{0.5}\}$ |
| Valve Closed | 0 | $Nu_4 = K_4\{0.022\ \overline{Re}_D^{0.8}\}$ |

From fit to data,

$K_1 = 0.40, \quad n = 0.6$

$K_2 = 1.0$

$K_3 = 0.4$

$K_4 = 1.0$

Note: The constants $C_1$ and $C_2$ were not adjustable and were determined from the literature [11,16]. These constants were a function of exhaust port Reynolds number and axial position [6].

Figure 9 shows the results for the time period model (solid curve) and for the measurement (dashed curve) for the port exit exhaust gas temperature for the four engine conditions considered previously. Good agreement in both temperature profile and absolute levels was obtained. The time-period model produced an improvement relative to the simple empirical model. These results are in agreement with the contention [14] that two dominant flow patterns exist during the exhaust valve open period.

Table 3 lists the complete set of correlations for the time-period model. Also listed is the fit coefficients for each correlation. The fit coefficient for the intermediate time period (pipe flow) was unity which indicates that the heat-transfer process was dominated by wall generated turbulence during this period.

Although this time-period model provided good results, the details of the model are not unique. Other combinations of the fundamental sub-models also produced similar agreement with the data. The time-period model described in this section, however, provided good agreement with the data with a minimum of detail and empirical constants.

*Effect of engine operation*

To facilitate the comparison of measured and computed gas temperatures, averaged temperatures were calculated from the time-varying quantities. An enthalpic average temperature was defined [7].

$$\bar{T}_i = \int_{EVO}^{EVC} \dot{m} C_P T_i \, dt \Big/ \int_{EVO}^{EVC} \dot{m} C_P \, dt. \qquad (20)$$

For constant $C_P$, equation (20) results in a mass-averaged temperature. This calculation was performed for the computed cylinder temperatures and for the computed and measured port exit temperatures using the computed mass flow rates at the valve and at the port exit, respectively. Figure 10 shows the results of these calculations as a function of engine operating conditions. The computed values are designated by the circles and solid lines and the experimental values are designated by the squares and dashed lines. Table 4 lists the computed mass-averaged temperatures and the computed residual fractions.

In general, the agreement with respect to engine operation was excellent for both trends and absolute values. The exhaust gas temperature reduction due to the port heat transfer was nominally about 200 K and

Table 4. Computed and measured results

| Parameter varied | $\bar{T}_C$ (K) | f (%) | $\bar{T}_{PX}$ (K) | $\bar{T}_{PC}$ (K) |
|---|---|---|---|---|
| Base | 1027 | 10.1 | 810 | 823 |
| IMEP=276 kPa | 997 | 13.1 | 824 | 803 |
| IMEP=621 kPa | 1053 | 7.6 | 901 | 854 |
| RPM=1300 | 1141 | 9.9 | 871 | 909 |
| RPM=1600 | 1155 | 9.7 | 889 | 936 |
| $\phi$ = 1.0 | 1034 | 10.4 | 839 | 833 |
| $\phi$ = 1.4 | 938 | 10.3 | 767 | 768 |
| $\theta_{SR}$ = -20° | 981 | 9.5 | 846 | 799 |
| $\theta_{SR}$ = 0° | 1062 | 10.8 | 831 | 840 |
| $\theta_{SR}$ = +15° | 1181 | 9.7 | 898 | 906 |

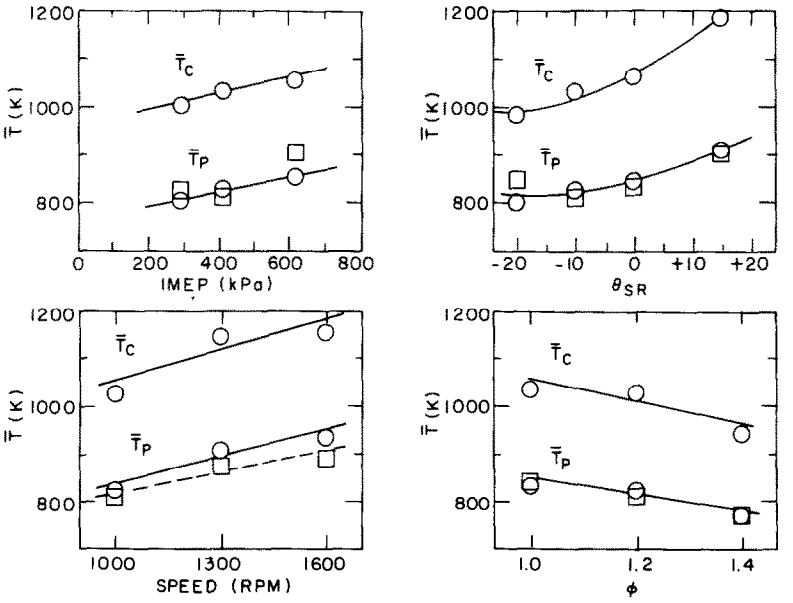


FIG. 10. Mass-averaged computed (circles) and measured (squares) cylinder and port exit temperatures as a function of engine load, speed, spark timing and equivalence ratio.

increased slightly with increases in mean temperature levels. The agreement was less satisfactory for the high load case and the most advanced timing case, due to low computed cylinder gas temperatures.

*Model sensitivity*

For the base engine operating condition, the model sensitivity was examined for three cylinder heat-transfer assumptions: (1) no heat transfer (adiabatic case), (2) the boundary-layer model and (3) Woschni's correlation [12]. These assumptions were fundamentally different; yet, the resulting temperatures were only moderately different [6]. During the blow-down flow period, the computed port exit temperatures were at most $\pm 2\%$ different. During the displacement flow period, the effect of the cylinder heat-transfer assumption was about $\pm 6\%$. This lack of sensitivity provided justification for the proposed port heat transfer model regardless of the cylinder heat-transfer assumption.

The modelling results were also examined for different assumptions of the port wall temperature [6]. For a 100 K variation in the wall and valve surface temperatures for the base engine operating condition, the predicted port exit temperature varied by about $\pm 5\%$. These results demonstrated only a slight sensitivity to the surface temperatures mainly due to the relatively large temperature difference between the gas and wall.

## SUMMARY AND CONCLUSIONS

Instantaneous heat-transfer models were developed for the exhaust port flow. Several fundamental submodels were examined to determine the dominant heat-transfer processes. An initial consideration was the empirical correlation of heat transfer in a pipe for turbulent flow. Even with the effects of developing flow and roughness included, this correlation underestimated the heat loss by more than a factor of 2. An order-of-magnitude analysis for the heat transfer due to large-scale fluid motion, on the other hand, yielded a correlation which estimated the heat transfer within about 20%. A purely empirical correlation [equation (19)] based on the form developed by the order-of-magnitude analysis produced good overall agreement with the data.

Since no single mode of heat transfer would, necessarily, dominate during the entire exhaust valve open period, combinations of the previously described submodels were examined. A time-dependent heat-transfer model, based on distinct flow regimes, was developed which consisted of four separate submodels. This correlation provided the best overall agreement with the data.

In addition, heat transfer to the exhaust valve in the port was also examined. Heat transfer to the valve back and valve stem was treated by adapting an empirical correlation for the heat transfer due to a two-dimensional jet impingement flow. The resulting correlation for the valve back and stem produced heat-transfer levels which were consistent with the assumption that the flow directed at the valve could be modelled as statnation flow. The separate treatment of the valve heat transfer was abandoned, however, because the resulting correlation was similar to the large-scale motion correlation. This similarity allowed a single correlation to be used for all surfaces.

*Acknowledgement*—This work was supported by a research grant from General Motors Research Laboratories, Warren, MI. The first author (JAC) was supported by a General Motors Fellowship.

## REFERENCES

1. J. A. Caton and J. B. Heywood, Models for heat transfer, mixing and hydrocarbon oxidation in an exhaust port of a spark-ignited engine, SAE Paper 800290 (1980).
2. D. R. Lancaster, R. B. Krieger and J. H. Lienesch, Measurement and analysis of engine pressure data, SAE Paper 750026 (February 1975).
3. R. S. Benson and G. W. Brundrett, Development of a resistance wire thermometer for measuring transient temperatures in exhaust systems of internal combustion engines, in *Temperature—Its Measurement and Control in Science and Industry*, Vol. III, Part 2, pp. 631–653. Reinhold, New York (1962).
4. R. S. Benson, Measurement of transient exhaust temperatures in I.C. engines, *The Engineer*, 376–383 (February 1964).
5. D. W. Wendland, The effect of periodic pressure and temperature fluctuations on unsteady heat transfer in a closed system, NASA-CR-72323 (March 1968).
6. J. A. Caton, Heat transfer, mixing and hydrocarbon oxidation in an engine exhaust port, M.I.T., Ph.D. Thesis (September 1979).
7. J. B. Heywood, J. M. Higgins, P. A. Watts and R. J. Tabaczynski, Development and use of a cycle simulation to predict SI engine efficiency and $NO_x$ emissions, SAE Paper 790291 (February 1979).
8. S. D. Hires, A. Ekchian, J. B. Heywood, R. J. Tabaczynski and J. C. Wall, Performance and $NO_x$ emissions modelling of a jet ignition prechamber stratified charge engine, SAE Paper 760161 (February 1976).
9. R. S. Spindt, Air-fuel ratios from exhaust gas analysis, *SAE Trans.* **74**, 788–793 (1965).
10. M. K. Martin and J. B. Heywood, Approximate relationships for the thermodynamic properties of hydrocarbon—air combustion products, *Combust. Sci. Technol.* **15**, 1–10 (1977).
11. W. M. Rohsenow and H. Y. Choi, *Heat, Mass and Momentum Transfer*. Prentice Hall, Englewood Cliffs, NJ (1961).
12. G. Woschni, A universally applicable equation for the instantaneous heat transfer coefficient in the internal combustion engine, *SAE Trans.* **76**, 3065–3083 (1968).
13. R. H. Sherman and P. N. Blumberg, The influence of induction and exhaust processes on emissions and fuel consumption in the spark ignited engine, SAE Paper 770990 (September 1977).
14. W. J. D. Annand and G. E. Roe, *Gas Flow in the Internal Combustion Engine*. G. T. Foulis, Sparkford, England (June 1974).
15. L. J. Danis, Engine valve cooling, SAE Paper 730055 (January 1973).
16. L. M. K. Boelter, G. Young and H. W. Iversen, An investigation of aircraft heaters. XXVII—Distribution of heat-transfer rate in the entrance section of a circular tube, NACA Technical Note No. 1451 (July 1948).
17. K. Tanka, Airflow through exhaust valve of conical seat, in *Proceedings of Third International Congress for Ap-*

*plied Mechanics*, Vol. 1, pp. 287–295 (1931).
18. J. W. Harrington, Visualization of the flow of exhaust through an internal combustion engine exhaust port, B.S.M.E. Thesis, MIT (May 1979).
19. B. B. Mikic, Personal communication (March 1979).
20. J. P. Holman, *Heat Transfer*, 2nd ed. McGraw-Hill Book, New York (1968).
21. R. Gardon and J. C. Akfirat, Heat transfer characteristics of impinging two-dimensional air jets, *J. Heat Transfer* **88**, 101–108 (1966).
22. A. Stotter, K. S. Woolley and E. S. Ip, Exhaust valve temperature—a theoretical and experimental investigation, SAE Paper 650019 (January 1965).
23. R. A. Seban and E. F. McLaughlin, Heat transfer in tube coils with laminar and turbulent flow, *Int. J. Heat Mass Transfer* **6**, 387–395 (1963).
24. J. H. Rush, Exhaust port heat rejection in a piston engine—a preliminary report, SAE Paper 760766 (October 1976).
25. G. S. Dreitser, E. K. Kalinin and V. A. Kuzminov, Transient convective heat transfer during various modes of cooling a hot gas in pipes, *J. Engng Phys.* **25**, 951–957 (1973).
26. V. V. Manayev, V. S. Nosov and N. I. Syromyatnikov, Investigation of heat transfer in pulsed flow of air in pipes, *Heat Transfer—Soviet Res.* **8**(3), 111–116 (May–June 1976).
27. G. F. Robertson, A study of thermal energy conservation in exhaust pipes, SAE Paper 790307 (February 1979).
28. R. D. Richtmyer, *Difference Methods for Initial-Value Problems*. Interscience, New York (1957).
29. V. S. Arpaci, *Conduction Heat Transfer*. Addison-Wesley, Reading, MA (1966).
30. S. D. Hires and G. L. Pochmara, An analytical study of exhaust gas heat loss in a piston engine exhaust port, SAE Paper 760767 (October 1976).
31. G. L. Malchow, S. C. Sorenson and R. O. Buckius, Heat transfer in the straight section of an exhaust port of a spark ignition engine, SAE Paper 790309 (February 1979).

## UNE ETUDE EXPERIMENTALE ET ANALYTIQUE DU TRANSFERT THERMIQUE A L'ORIFICE DE SORTIE D'UN MOTEUR

**Résumé**—A cause d'un besoin croissant d'information précise sur le fonctionnement d'un moteur, on développe une étude et on vérifie expérimentalement des modèles sur le transfert de chaleur instantané à l'échappement d'un cylindre. Des mesures de la pression instantanée dans le cylindre et de la température instantanée à l'échappement sont effectuées pour un domaine de conditions de fonctionnement d'un moteur. Les mesures de pression permettent d'atteindre l'état instantané du gaz dans le cylindre et les mesures de température permettent de valider les modèles de transfert thermique.

Le transfert à l'échappement est dominé par un mouvement de jet à large échelle au contraire du mouvement de fluide à frottement pariétal. Une analyse basée sur la vitesse du jet à travers l'ouverture de la soupape prédit correctement le transfert de chaleur dû à ce mouvement à grande échelle. Des modèles pour l'échappement instantané fournissent un accord excellent avec des mesures pour les conditions de fonctionnement du moteur.

## EINE EXPERIMENTELLE UND ANALYTISCHE UNTERSUCHUNG DES WÄRMEÜBERGANGES IN EINER MOTOR-AUSLASS-ÖFFNUNG

**Zusammenfassung**—Wegen des zunehmenden Bedarfs an genauer Information über Verbrennungsmotoren-Prozesse wurden in dieser Studie Modelle für den momentanen Wärmeübergang in einer Motor-Auslaß-Öffnung entwickelt und experimentell bestätigt. Die Momentanwerte des Zylinderdrucks und der Abgastemperatur wurden in Versuchen für einen ausgedehnten Betriebsbereich gemessen. Druckmessungen wurden verwendet, um den momentanen Gaszustand im Zylinder zu bestimmenn und Temperaturmessungen dienten zur Bestätigung der Wärmeübergangs-Modelle.

Der Wärmeübergang in der Auslaß-Öffnung wurde im wesentlichen durch die strahlinduzierte Makro-Bewegung des Fluides entgegen der durch Wandschubspannung erzeugten Fluidbewegung bestimmt. Eine theoretische Untersuchung, die sich auf die Strahlgeschwindigkeit durch die Ventilöffnung stützt, liefert korrekt den Wärmeübergang, hervorgerufen durch diese Makro-Bewegung. Die Modelle für den momentanen Wärmeübergang in der Auslaß-Öffnung als Funktion der Arbeitsbedingungen des Motors zeigten vorzügliche Übereinstimmung mit den Messungen.

## ЭКСПЕРИМЕНТАЛЬНОЕ И АНАЛИТИЧЕСКОЕ ИССЛЕДОВАНИЕ ТЕПЛОПЕРЕНОСА В ВЫХЛОПНОМ ОТВЕРСТИИ ДВИГАТЕЛЯ

**Аннотация** — В связи с все более возрастающей необходимостью в точной информации о процессах, происходящих в двигателях, предложены модели теплопереноса в выхлопном отверстии двигателя. Измерялись давление в цилиндре и температура выхлопного газа при различных режимах работы двигателя. Данные по давлению использовались для определения состояния газа в цилиндре, а по температуре — для проверки справедливости предложенных моделей. Теплоперенос в выхлопном отверстии определяется крупномасштабными перемещениями жидкости, возникающими при струйном истечении, которые существенно отличаются от перемещений, вызываемых напряжением сдвига на стенке. Анализ, основанный на скорости истечения струи через отверстие клапана, позволяет корректно оценить величину теплового потока при таких крупномасштабных перемещениях. Модели теплопереноса в выхлопном отверстии хорошо согласуются с результатами измерений при различных режимах работы двигателя.